Experimental Behavior of Steel Fiber Reinforced Concrete Deep Beams

F.B.A. Beshara[a], A. A. Mahmoud[b] and A. A. El-Barbary[c]

[a, b, and c] *Department of civil engineering, faculty of engineering (Shoubra), Benha University, Shoubra, Cairo, Egypt*

Abstract. This paper presents an experimental investigation on high strength steel fiber reinforced concrete (HSSFRC) deep beams behavior under monotonic static loads. Eleven simply-supported deep beams were tested and divided into three groups with different structural parameters. The studied factors were steel fiber volume fractions (V_f), fibers aspect ratios (l_f/ϕ_f), and shear span-to-depth ratios (a/d). The mean compressive strength of concrete is 60 MPa. The main objectives were to study the effect of fibers inclusion on response characteristics such as the shear carrying capacity, load-deflection curves, load-steel strain relationships, concrete surface strains, and failure modes. The testing results indicated that (a/d) ratio has a significant effect on the behavior of deep beams. Also, load carrying capacity, stiffness and strain ductility increase considerably with the increase of (V_f) or (l_f/ϕ_f) ratio.

Keywords: Shear strength, high strength concrete, deep beams, and steel fibers.

1. INTRODUCTION

Deep beams are structural members used in high rise buildings as transfer girders, in foundation as walls and as pile caps, and in water structures as walls of tanks. There have been extensive experimental programs to study the behavior and failure mechanisms of reinforced concrete deep beams; e.g. [1-3]. Due to the low ductility and brittleness of high strength concrete, adding discontinues steel fibers embedded in concrete matrix can provide the required ductility. Many reports published over the past four decades e.g. [4, 5] confirm that the use of randomly oriented discrete short steel fibers is effective in overcoming the brittleness of high strength concrete. In the literature, available investigations; e.g. [1, 6-8] are reported for the behavior of normal strength fiber concrete deep beams where the role of fiber volume, fiber aspect ratio and fiber types was studied. Very few studies are performed on high strength steel fiber reinforced concrete deep beams [9, 10]. In the present work, the results of an experimental program [11] are reported to study the influence of steel fibers inclusion on the behavior of high strength fiber concrete deep beams.

2. DESCRIPTION OF EXPERIMENTAL PROGRAM

The test specimens included eleven simply-supported deep beams with constant cross section of total depth 500 mm and width 120 mm. The overall dimensions of typical specimens are shown in Fig. 1 and in Table 1. The provided flexural and shear reinforcement were chosen to satisfy the requirements of the Egyptian Code [12]. The specimens were reinforced longitudinally by (2ϕ18mm) and (2ϕ10mm) as main and secondary steel, respectively. The main reinforcement was high-tensile steel bars, while

the web reinforcement was mild steel bars with 8-mm diameter. The proof stress for longitudinal bars was 438 MPa and the yield stress for web steel was 299 MPa. For concrete, a trial mix design has been conducted to get characteristic compressive strength of standard cube as greater or equal 60 MPa. The specimens were divided into three main groups A, B and C with a shear span-to-depth ratio (*a/d*) equal to 0.44, 0.81 and 1.0 respectively, as given in Table 1. The specimens of these groups contain different fibers volume content V_f as 0.0%, 0.5% & 1.0%, and different fibers aspect ratio l_f/ϕ_f as 60 & 80.

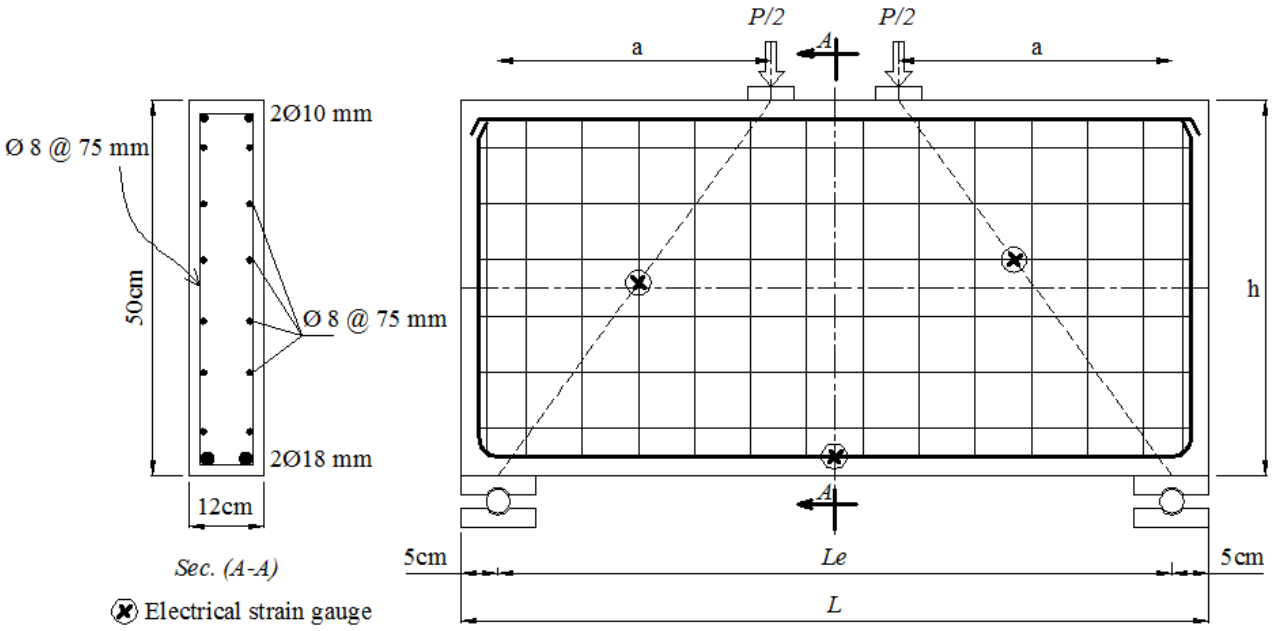

FIGURE 1. Geometrical dimensions of the tested deep beams

TABLE 1. Details of tested deep beams

Beam	*a* (mm)	L_e (mm)	*a/d*	V_f (%)	l_f/ϕ_f	S_v (mm)	ρ_v (%)	S_h (mm)	ρ_h (%)
A0	200	700	0.44	0.00	0	75	1.12	75	1.12
A1	200	700	0.44	0.50	80	75	1.12	75	1.12
A2	200	700	0.44	1.00	60	75	1.12	75	1.12
A3	200	700	0.44	1.00	80	75	1.12	75	1.12
B0	365	900	0.81	0.00	0	75	1.12	75	1.12
B1	365	900	0.81	0.50	80	75	1.12	75	1.12
B2	365	900	0.81	1.00	60	75	1.12	75	1.12
B3	365	900	0.81	1.00	80	75	1.12	75	1.12
C0	450	1000	1.00	0.00	0	75	1.12	75	1.12
C1	450	1000	1.00	0.50	80	75	1.12	75	1.12
C2	450	1000	1.00	1.00	80	75	1.12	75	1.12

The volumetric ratio of vertical ρ_v and horizontal ρ_h web steel for groups A, B and C was constant and equals 1.12%. The specimens were tested up to failure using a compression-testing machine of 5000 kN capacity and 0.10 kN accuracy. Each test specimen was connceted to the computer to record micro-strains, forces, and displacements. Each beam was laterally stiffened by four wooden arms ended by rubber wheel to prevent horizontal movement during loading as shown in Fig. 2. All results were recorded automatically using the data logger. Electrical strain gauges were used to measure the strains in concrete surface, and in the main longitudinal bottom steel. The vertical deflection of test beams at mid-span was measured using LVDT. The demec points were used to draw the surface concrete strain distribution along the beam depth. The distance between each couple of demec points were 100 mm.

FIGURE 2. Test setup

3. OBSERVED BEHAVIOR AND FAILURE MODES

The loading increment began with 100 kN per each loading step and was reduced to be 50 kN after first crack. The flexural crack appeared earlier than the diagonal shear cracks. The first flexural crack was vertical and appeared in the flexural sagging region (mid-span) at approximately 37% of the ultimate strength. Then, the first crack in the diagonal direction appears approximately at 50% of ultimate strength. The shear cracks extended towards both the support and loading points; parallel to strut between points of loading and support. Further increase in load resulted in the propagation all cracks; and simultaneously, new diagonal cracks developed more or less parallel to the existing

ones. Some of these new cracks had originated vertically, but later become sloped in a diagonal direction. The influence of fiber content V_f and fiber aspect ratio (l_f/ϕ_f) is very sensitive; the increase of V_f or (l_f/ϕ_f) enhances the shear and tension resistances of concrete and plays an important role to bridge and arrest the cracks. This is the reason of delay of appearance of first flexural and diagonal shear cracks for fibrous deep beams. For all tested beams, the observed failure modes are summarized in Table 2. The observed failure modes for deep beams were namely shear-compression**,** diagonal-splitting and crushing of strut. Fig. 3 shows the various crack patterns and the different modes of failure. The first mode is shear-compression failure which is concerned with low *a/d* ratios such as beams A2 and A3; shown in Fig. 3-a. This mode of failure is brittle failure. The second mode is diagonal splitting which is less brittle (ductile) in a comparison with the first one. During the failure process, the ultimate load of fibrous beams was able to be maintained on the specimens despite wide cracks due to the post-cracking strength of steel fibers. Degradation of the load carrying capacity started with the pull-out or the rupture of fibers across the open cracks. At impending failure, some crushing of the concrete was observed between the loading points and the tip of the major inclined crack. This mode is related to high values of each V_f, l_f/ϕ_f and *a/d* ratios, such as beams B2 and C1 as shown in Fig. 3-b. During the cracking development process under load increasing for some specimens, the concrete strut between the inclined cracks failed in compression. This mode of failure is brittle and sudden and can be classified as crushing of strut failure such as beam C2 & A1 shown in Fig. 3-c.

TABLE 2. Expiremntal results of all specimens

Specimen	P_{crs} (kN)	$P_{u(EXP)}$ (kN)	Δ_y (mm)	Δ_u (mm)	$\phi_{\Delta u}$	Failure mode	Yield strain $\varepsilon_{y} \times 10^{-3}$	Ult. strain $\varepsilon_{u} \times 10^{-3}$	Failure strain $\varepsilon_{f} \times 10^{-3}$	Strain ductility $\phi_{\varepsilon f} = \varepsilon_f / \varepsilon_y$
A0	350	1150	1.80	2.56	1.4	S.C.(1)	1.90	2.00	2.10	1.11
A1	400	1350	1.46	2.22	1.5	C.S.(2)	2.08	2.08	2.50	1.20
A2	400	1380	1.21	2.11	1.7	S.C.(1)	2.12	2.11	2.86	1.35
A3	400	1420	0.96	1.68	1.7	S.C.(1)	2.20	2.14	3.08	1.40
B0	320	670	1.98	3.08	1.5	C.S.(2)	2.05	2.51	2.60	1.27
B1	400	703.0	1.50	2.58	1.7	D.S.(3)	2.10	2.59	2.75	1.31
B2	450	740.5	1.37	2.52	1.8	D.S.(3)	1.93	2.61	2.80	1.45
B3	450	781.0	1.14	2.43	2.1	D.S.(3)	2.15	2.64	3.24	1.51
C0	320	490.0	2.25	3.66	1.6	D.S.(3)	2.31	2.71	3.11	1.35
C1	300	550.0	1.69	3.35	1.9	D.S.(3)	2.28	2.77	3.24	1.42
C2	450	600.0	1.25	2.93	2.3	C.S.(2)	2.31	2.82	3.55	1.54

S.C. (1) (Shear compression failure) ;
C.S. (2) (Crushing of strut failure) ;
D.S. (3) (Daigonalplitting failure).

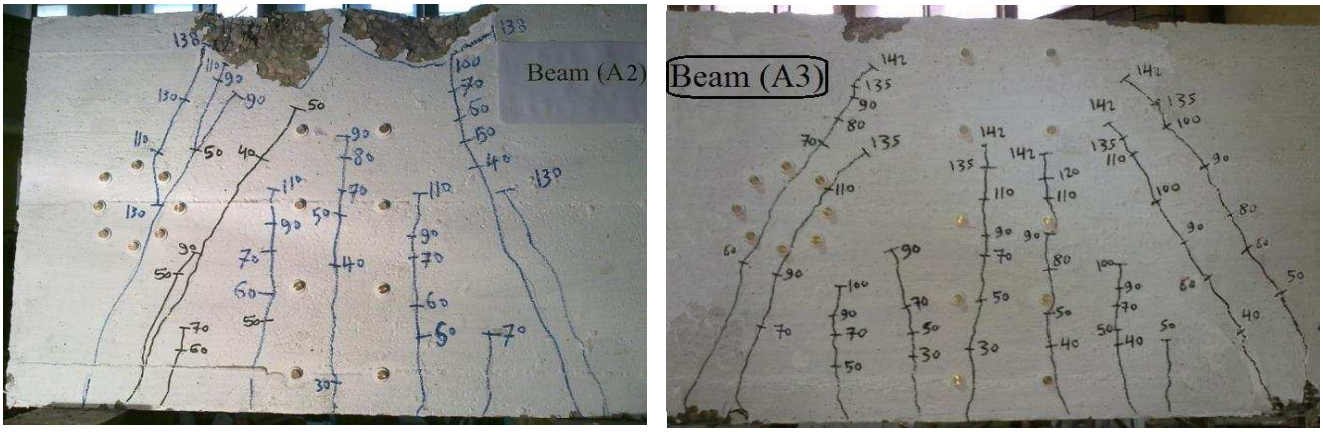

(a) Shear compression failure

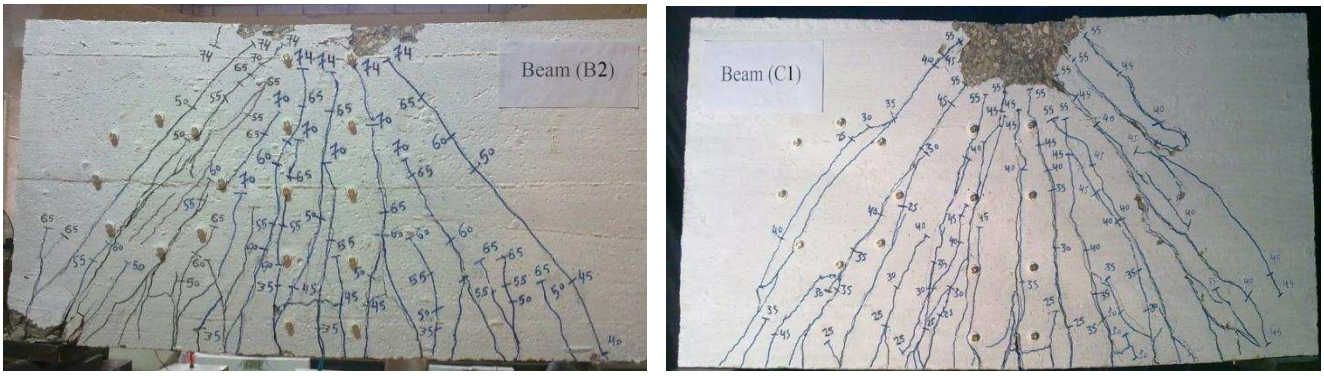

(b) Daigonal splitting failure

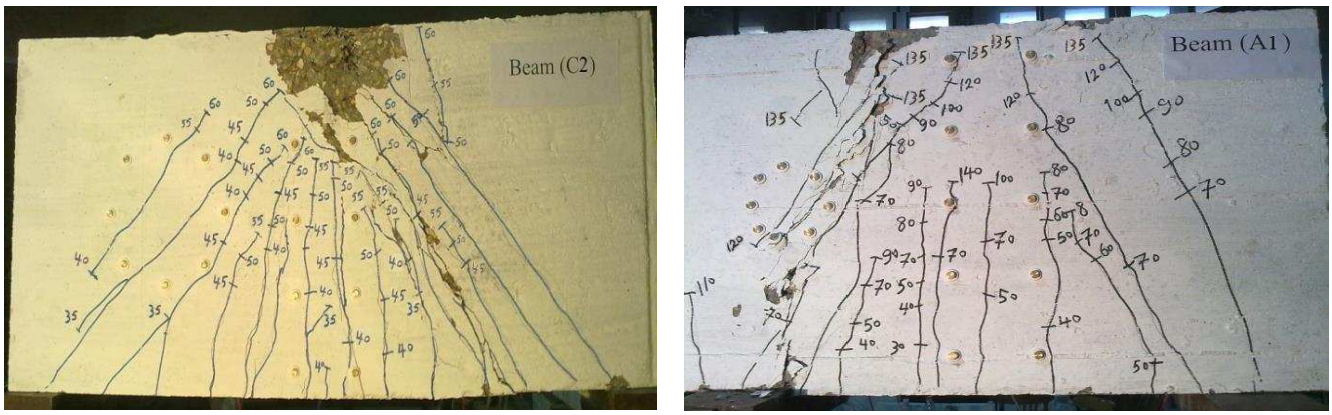

(c) Crushing of strut failure

FIGURE 3. Different modes of failure

4. MEASURED LOAD-DEFLECTION AT MID-SPAN

At early stages, the beams behaved in an elastic manner and the load-deflection relations were linear. After first diagonal cracking, the response is nonlinear and is characterized by a curvilinear manner. The measured load-deflection curves of tested beams were grouped in order to study the effects of testing variables. In Table 2, the experimental results are given for the measured first diagonal cracking load P_{crs}, the ultimate total load $P_{u(EXP)}$ and the deflections at the yield Δ_y and ultimate Δ_u levels.

The displacement ductility of each beam $\phi_{\Delta u}$, is also calculated as the ratio between displacement at ultimate to the yield displacement.

For different fiber contents (V_f = 0.0%, 0.5% & 1%), the measured load-deflection curves till failure are drawn in Fig.4-a for beams A0, A1 & A3 and in Fig. 4-b for beams C0, C1 and C2. Also, the effect of fiber aspect ratio (l_f/ϕ_f = 0.0, 60 & 80) on the measured load-deflection curves is plotted in Fig. 5-a for A0, A2 and A3 and in Fig. 5-b for beams B0, B2 and B3. From the results of these figures and Table 2, the increase of (V_f) or (l_f/ϕ_f) leads to an increase in the ultimate load carrying capacity $P_{u(EXP)}$ as a result of the enhanced post-cracking strength of steel fiber reinforced concrete. Also, the increase of (l_f/ϕ_f) ratio increases the pull-out resistance of fibers. As V_f increased from 0.0% to 1.0%, $P_{u(EXP)}$ was enhanced by 24%, 17%, and 23% for groups A, B, and C, respectively. The average increase in $P_{u(EXP)}$ is 21%. As l_f/ϕ_f ratio was increased from 0 to 80 with constant fiber content as 1%, $P_{u(EXP)}$ was higher by 23.5% for group A, by 14.2% for group B, and by 22.4% for group C. The mean increase in $P_{u(EXP)}$ is 20%. Also, the increase of (V_f) or (l_f/ϕ_f) delays the appearance of the first diagonal shear cracks, especially for deep beams with a/d > 0.44. For non-fibrous deep beams, the ratio between cracking shear load and ultimate load P_{crs}/P_{uEXP} was 0.48 in group B and 0.65 in group C. For constant l_f/ϕ_f as 80 in Group C, P_{crs}/P_{uEXP} ratio is 0.55 for V_f = 0.5% and 0.75 for V_f = 1.0%. For constant V_f as 1% in Group B, P_{crs}/P_{uEXP} ratio is 0.57 for l_f/ϕ_f = 60 and 0.58 for l_f/ϕ_f = 80.

The measured deflections indicate that beams with higher (V_f) or (l_f/ϕ_f) exhibit less deformation as the existence of steel fibers bridge and arrest the concrete cracks under applied stresses. As V_f increased from 0.0% to 1.0%, the final deflection was reduced by 34%, 21%, and 19% for groups A, B, and C, respectively. The average decrease in Δ_u is 25%. The growth of l_f/ϕ_f from 0 to 80 with V_f = 1%, results in a reduction of the final deflection Δ_u by 34.4% for group A, by 42.4% for group B, and by 20.0% for group C. The mean decrease in Δ_u is 32%. Also, the rise of fiber aspect ratio l_f/ϕ_f enhances the displacement ductility. As V_f increased from 0.0% to 1.0%, $\phi_{\Delta u}$ was increased by 23%, 37%, and 44% for groups A, B, and C, respectively. The average increase in $\phi_{\Delta u}$ is 35%. The rising of (l_f/ϕ_f) from 0 to 80 increases $\phi_{\Delta u}$ by 23.2% for group A, by 36.5%, for group B, and by 43.6% for group C. The mean increase in $\phi_{\Delta u}$ is 34%. For different values of shear span-to-depth ratio a/d, the measured load-deflection curves are drawn in Fig. 6-a for beams A1, B1 and C1 and in Fig. 6-b for beams A3, B3 and C2. These figures indicate that the decrease of (a/d) ratio leads to an increase in the load carrying capacity at different levels as a result of enhanced arching action. As (a/d) ratio decreased from 1.00 to 0.44, the ultimate load carrying capacity was increased by 70%. Also, the first diagonal shear crack load was increased by 25%. The measured deflections indicate that beams with smaller (a/d) ratio exhibit less deformation. As a/d ratio decreased from 1.00 to 0.44, the deflection at failure load was decreased by average 61%. The degree of displacement ductility varied depending on a/d ratio; the lower a/d ratio the lower amount of displacement ductility. As a/d ratio decreased from 1.00 to 0.44, $\phi_{\Delta u}$ was decreased by average 56%.

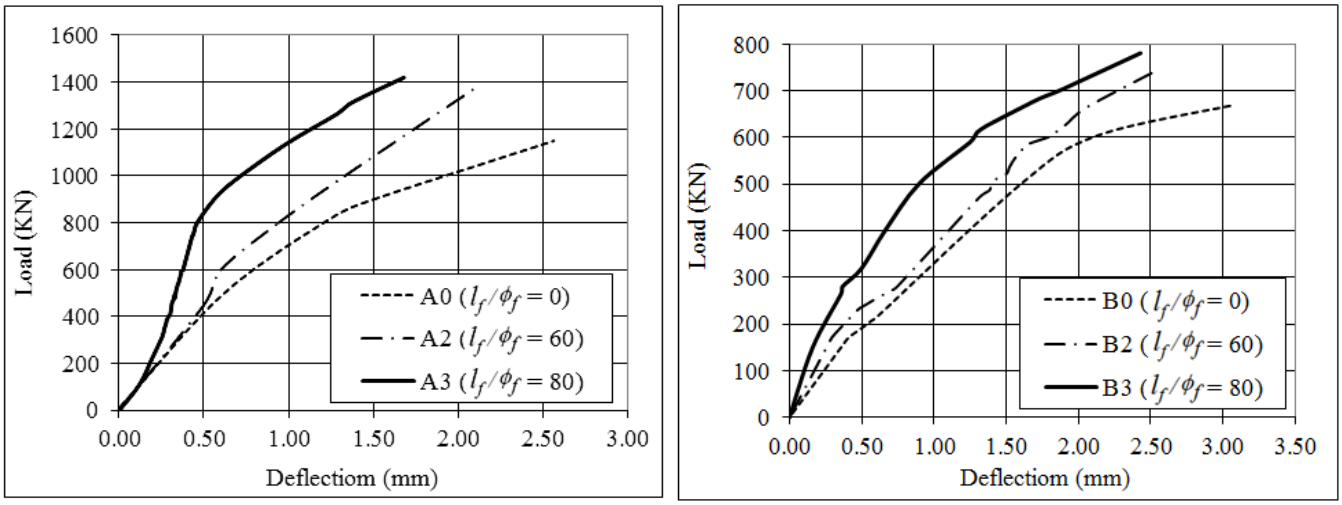

(a) a/d =0.44 & V_f = 1.0 (b) a/d =0.81 & V_f = 1.0

FIGURE 5. Effect of fiber aspect ratio (l_f/ϕ_f) on structural response

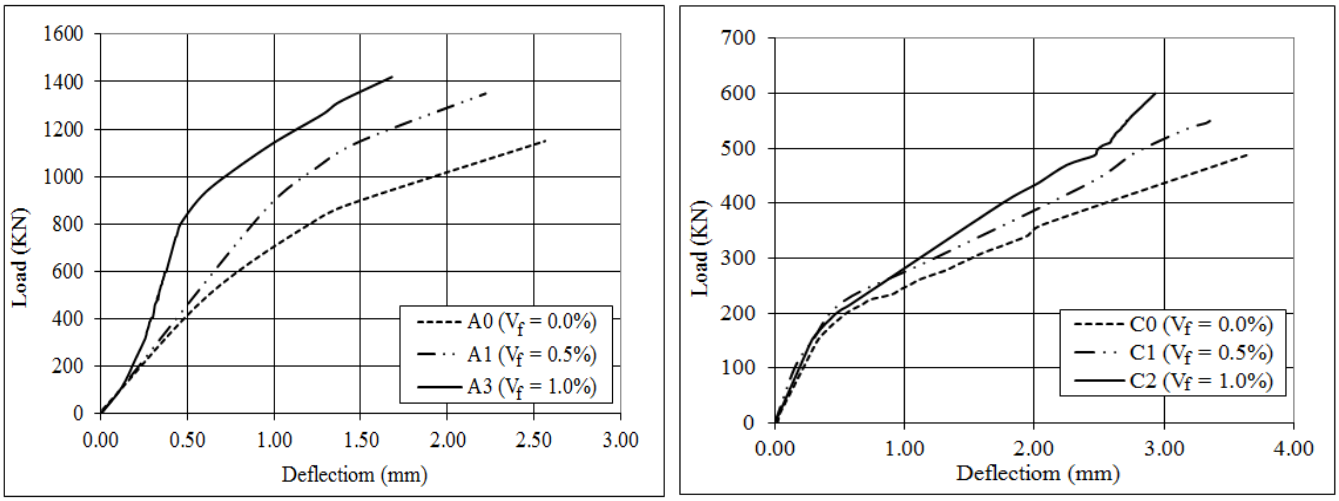

(a) a/d =0.44 & l_f/ϕ_f = 80 (b) a/d =1.00 & l_f/ϕ_f = 80

FIGURE 4. Effect of fiber volume content (V_f) on structural response

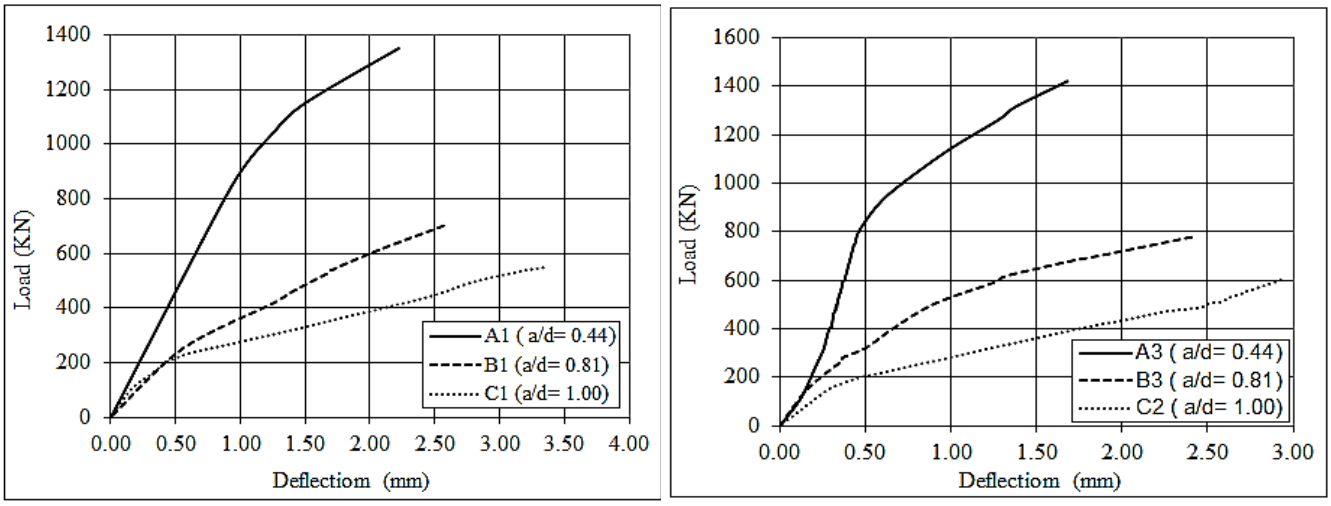

(a) V_f = 0.5 & l_f/ϕ_f = 80 (b) V_f = 1.0 & l_f/ϕ_f = 80

FIGURE 6. Effect of shear span -to-depth ratio (a/d) on structural response

5. MEASURED STEEL AND CONCRETE STRAINS

For all beams, the strain results of longitudinal main steel are given in Table 2 at yield level ε_y, at ultimate level ε_u, and at failure ε_f. Also, the displacement ductility of critical beam section $\phi_{\varepsilon f}$ is given and calculated as the ratio between the strain at failure and the yield strain. Fig. 7-a and Fig. 7-b show the effect of fiber volume on measured load-steel strain curves for beams A0, A1 and A3 and for beams C0, C1 and C2, respectively. The effect of fiber aspect ratio l_f/ϕ_f on the measured load-steel strain response is illustrated in Fig. 8-a for beams A0, A2 and A3, and in Fig. 8-b belong to beams B0, B2 and B3. It is clear that increasing the fiber volume or the fiber aspect ratio has a minor effect on the improvement of the ascending branch of measured curves of tested beams. The slight increase in the slope for curves with higher V_f or l_f/ϕ_f is due to the enhanced tension stiffening effect due to fibers inclusion.

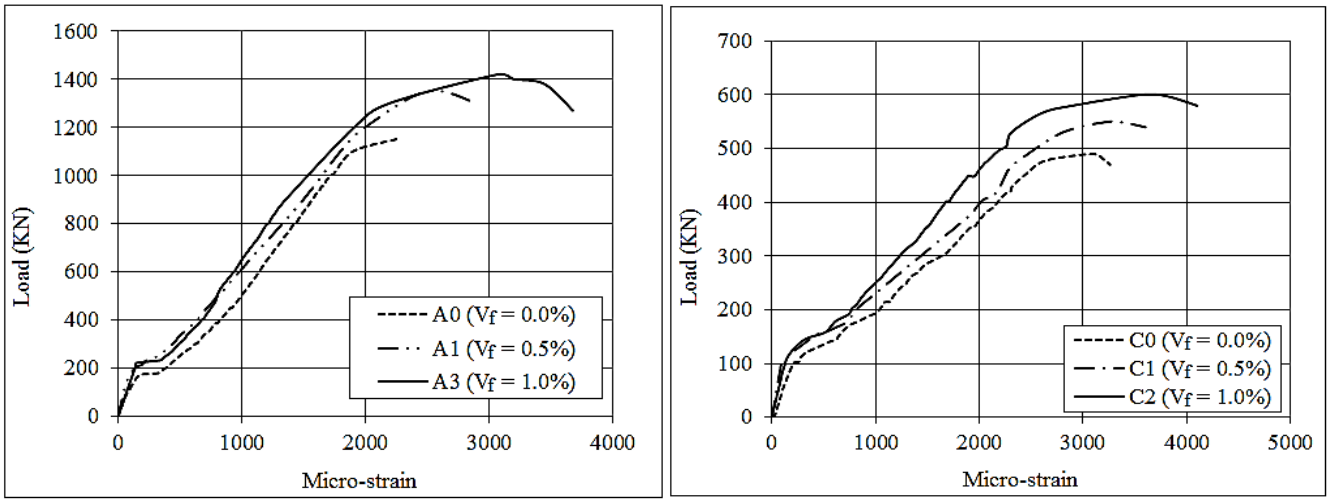

(a) a/d = 0.44 & l_f/ϕ_f = 80 (b) a/d = 1.00 & l_f/ϕ_f = 80

FIGURE 7. Effect of fiber volume content (V_f) on the load- steel strain response

The effect of increasing V_f or l_f/ϕ_f is mainly clear in the post-yield regime. As V_f increased, the steel strain at ultimate load level was increased, and displacement ductility was increased too. The effect of shear span-to-depth ratio *a/d* is studied in Fig. 9-a for beams A1, B1 and C1 and in Fig. 9-b for beams A3, B3 and C2. The decrease of (*a/d*) ratio leads to decreasing the tensile strain in steel at different load levels. As expected the increase of (*a/d*) ratio increases the flexural effect and consequently increases the steel strain and displacement ductility. Due to the enhanced arching action effect, the slope of the load-steel strain curves is significantly increased for beams with lower (*a/d*) ratio.

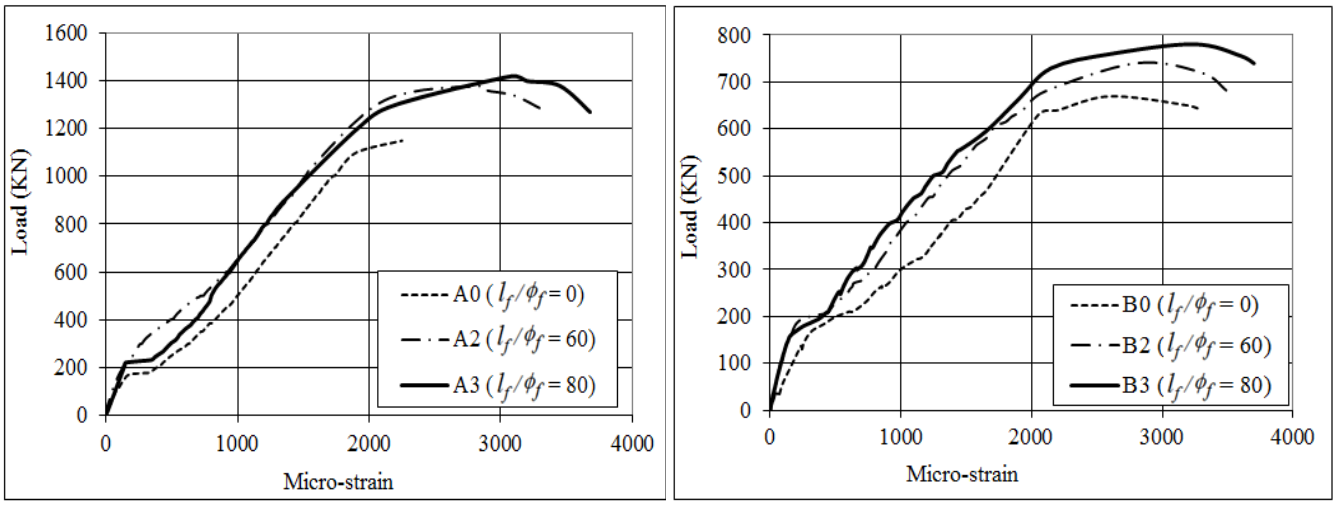

(a) a/d = 0.44 & V_f = 1.0 (b) a/d = 0.81 & V_f = 1.0

FIGURE 8. Effect of fiber aspect ratio (l_f/ϕ_f) on the load- steel strain response

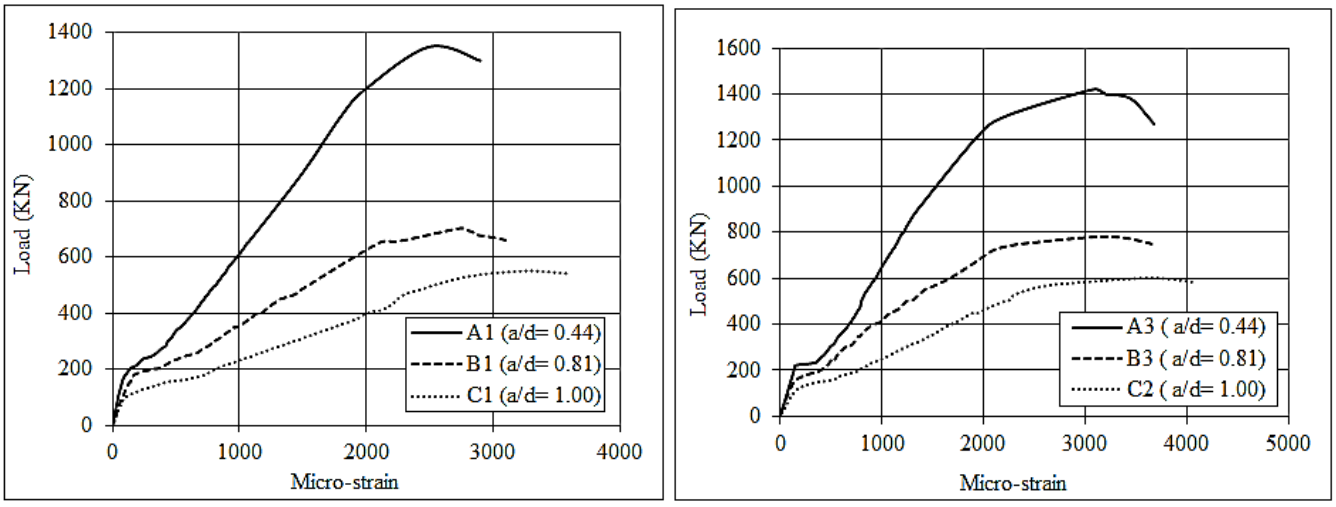

(a) V_f= 0.5 & l_f/ϕ_f= 80 (b) V_f= 1.0 & l_f/ϕ_f= 80

FIGURE 9. Effect of shear span -to-depth ratio (*a/d*) on the load- steel strain response

Typical strain distribution profiles for some beams are drawn in Fig. 10. These profiles were drawn for mid-span critical sections at 80% of ultimate load. The strain distribution is nonlinear. The compression strain at the top fiber of mid span section increases as the load increases, but in the tension zone the various recorded values were disturbed by the cracks and the flexibility of this area. The concrete strain measurements in the tension zone are not accountable and steel strain is only governed. The neutral axis has a changeable depth till the failure. The upward movement of neutral axis is associated with the cracking progress under load increase.

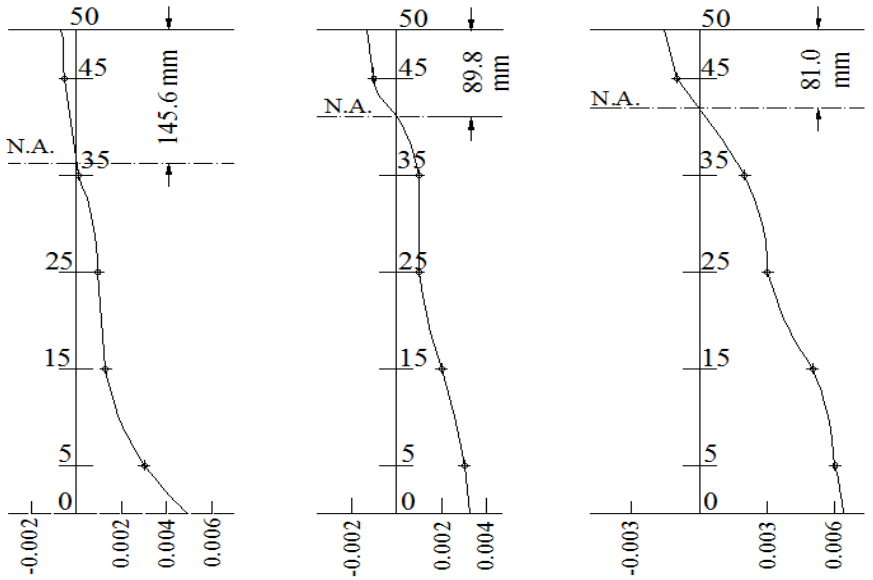

Beam (A1) Beam (B1) Beam (C1)

FIGURE 10. Typical strain distribution profiles for some specimens

6. COMPARISON WITH ANSYS PROGRAM RESULTS

Using ANSYS program, nonlinear finite element analysis was performed [11] for the deep beams. For beams A1, B2, A2, and C2, comparative studies are shown in Fig. 11. The predicted numerical results for loading and deflection at ultimate and first cracking levels result, show a good agreement with the experimental results.

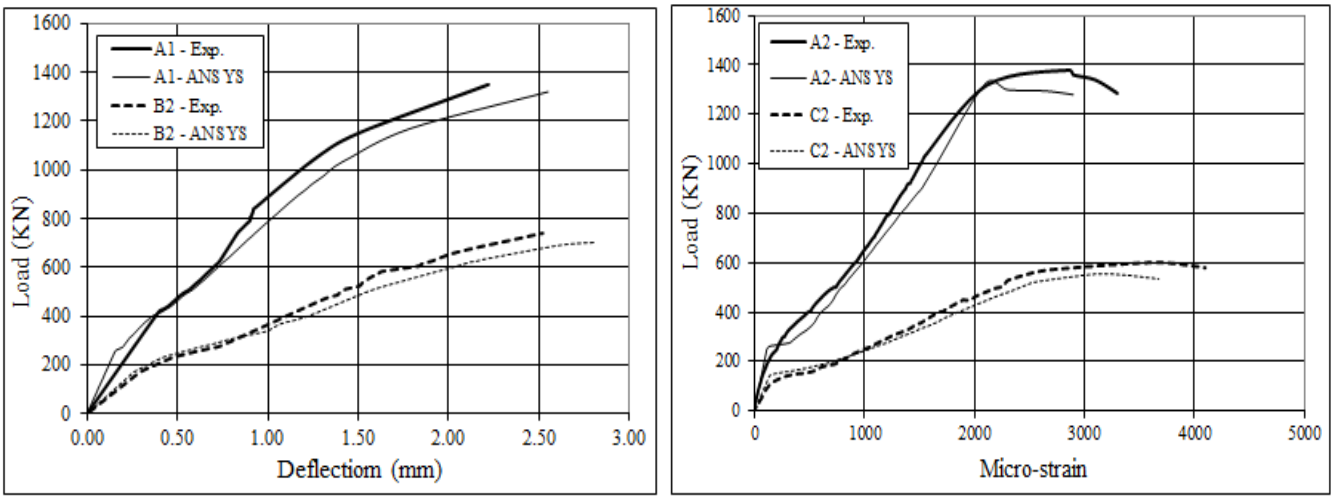

(a) (b)

FIGURE 11. Comparative Studies between Experimental and Numerical Predictions

Also, the simulated cracking patterns and failure modes are nearly similar to the testing results. The average ratio between measured load and predicted load is 0.91 at first diagonal crack level, and 1.1 at ultimate level. Finally, the mean ratio between numerical and experimental ultimate deflection values is 1.12%.

7. CONCLUSIONS

From the testing results of present work, the following conclusions are drawn:

1. Generally, the failure modes of all specimens are shear accompanied with clear vertical and diagonal cracks. The failure modes for deep beams without fibers were sudden brittle failure modes; namely shear-compression and crushing of strut. As fiber volume content V_f and fiber aspect ratio l_f/ϕ_f is increased, the mode of failure changes to less brittle failure mode which is called diagonal-splitting failure mode. Also, the strain distribution profiles are nonlinear for all specimens.

2. The increase in fiber volume content V_f or fiber aspect ratio l_f/ϕ_f leads to an increase in ultimate load $P_{u(EXP)}$, in first diagonal cracking load P_{crs}, and in displacement ductility $\phi_{\Delta u}$ while it reduces the ultimate deflection Δ_u. For fiber content V_f = 1%, the average increase in $P_{u(EXP)}$, P_{crs}, and $\phi_{\Delta u}$ was 21%, 32% and 35% , respectively. The mean reduction in Δ_u was 25%. The change of fiber aspect ratio l_f/ϕ_f from zero to 80 rises P_{crs} by 32%, $P_{u(EXP)}$ by 4% and $\phi_{\Delta u}$ by 34%, while it reduces Δ_u by 12%. As fiber volume V_f increased, the steel strain corresponding to ultimate load was increased, and $\phi_{\Delta u}$ was increased too.

3. The decrease of shear span-to-depth ratio *a/d* enhances the ultimate load carrying capacity and first diagonal crack P_{crs}, while it reduces the displacement ductility $\phi_{\Delta u}$ and the ultimate deflection Δ_u. This improvement is due to the enhanced arching action effect. The change of *a/d* ratio from 1.00 to 0.44 increases $P_{u(EXP)}$ by 70%, rises P_{crs} by 25%, reduces $\phi_{\Delta u}$ by 56% and decreases Δ_u by 61%. The decrease of *a/d* ratio leads to decreasing the tensile strain in steel at different load levels.

REFERENCES

1. **Kong F. G.,** "Reinforced concrete deep beams", 2nd ed., Taylor & Francis, **2003.**
2. **Michael D. B., and Bayrak O.,** "Investigation of deep beams with various load configurations", ACI Struct. J., V.104, No.5, **2007,** pp. 611-620.
3. **Mihaylov B. I., Hunt B., Bentz E. C., and Collins M. P.,** "Three-parameter kinematic theory for shear behavior of continuous deep beams", ACI Struct. J., V.112, No. 1, **2015,** pp. 47-58.
4. **Bentur A., and Sidney M.,** "Fiber reinforced cementitious composites", 2nd ed., Elsevier applied science, London and New York, **1990.**
5. **ACI Committee 544,** "Design Considerations for Steel Fibers Reinforced Concrete", ACI 544. 4R- 88, ACI Struct. J., V.96, No.5, **1999,** pp.563-580.
6. **Narayanan R., and Darwish, I. Y. S.,** "Fiber concrete deep beams in shear", ACI Struct J., V.85, No.2, **1988,** pp. 141-149.
7. **Mansur, M. A., and Ong, K. C. G.,** "Behavior of Reinforced Fiber Concrete Deep Beams in Shear", ACI Struct. J., V.88, No.1, **1991,** pp.98-105.
8. **Campione, G.,** "Flexural behavior of steel fibrous reinforced concrete deep beams", J. Struct. Eng., ASCE, V.138, No.2, **2012,** pp. 235-246.
9. **Padmarajaiah, S. K., and Ramaswamy A.,** "Behavior of fiber-reinforced prestressed and Reinforced high-strength concrete beams subjected to shear", ACI Struct. J., V.98, No.5, **2001,** pp. 752-761.
10. **Naik, U. P., and Kute, S.,** "Effect of shear span to depth ratio on shear strength of steel fiber reinforced high strength concrete deep beam", International J. of Advanced Struct. Eng., V.29, No.5, **2013,** pp. 1-12.
11. **El-barbary, A. A.,** "Performance of steel fibers reinforced concrete deep beams", Ph.D. thesis, Faculty of Engineering, Shoubra, Benha University, Egypt, **June 2015.**
12. **Housing and building research center,** "Egyptian code of practice for design and construction of Reinforced concrete structures", Egypt, **2012.**